



An efficient deep learning scheme to detect breast cancer using mammogram and ultrasound breast images

Adyasha Sahu ^{a,*}, Pradeep Kumar Das ^b, Sukadev Meher ^a

^a Department of Electronics and Communication Engineering, National Institute of Technology Rourkela, Odisha, 769008, India

^b School of Electronics Engineering (SENSE), Vellore Institute of Technology Vellore, Tamil Nadu, 632014, India



ARTICLE INFO

Keywords:

Deep learning
Breast cancer
Mammogram
Ultrasound
Transfer learning
Classification

ABSTRACT

Breast cancer is the second major reason of death among women around the world. Early and accurate breast cancer detection is important for proper treatment planning to save a life. In this paper, a deep learning-based ensemble classifier is proposed for the detection of breast cancer. The primary contributions are: (1) an efficient deep learning-based breast cancer detection method that can exhibit admirable performance with a small dataset; (2) the integration of three efficient transfer learning models (AlexNet, ResNet, and MobileNetV2), which lead to more accurate results; (3) the use of residual learning, depthwise separable convolution, and inverted residual bottleneck structure to make the system faster, as well as skip connection to make optimization easier and lastly, employing Laplacian of Gaussian (LoG) and modified high-boosting to improve performance. The experimental results convey that the suggested scheme gives superior classification performance by achieving an accuracy of 99.17% to detect abnormality and 97.75% to detect malignancy on the mini-DDSM dataset. Similarly, on the ultrasound dataset (BUSI), it provides accuracies of 96.92% and 94.62% to detect abnormality and malignancy, respectively. It also gives the best performance in another ultrasound dataset, BUS2, with 97.50% accuracy. Therefore, because of its versatility and reliability, the proposed model can be used for breast cancer detection in multimodal datasets.

1. Introduction

Breast cancer is a type of cancer mostly seen among women. It is the uncontrolled and irregular growth of breast tissues forming a lump or tumor [1,2]. These breast lesions are of two types: benign and malignant. A benign breast tumor grows slowly and does not infect the nearby cells, whereas a malignant breast tumor grows very fast and infects the neighboring cells very quickly [3]. Generally, breast cancers are lobular or ductal. Lobular cancer originates from the lobule or the gland that produces milk, whereas ductal cancer originates from the duct or the milk-carrying tube to the nipple.

There are some common threat factors of breast cancer; some of them, which are controllable, are less physical activity, obesity, and consumption of alcohol, whereas the uncontrollable factors are: genetics, early menstruation, and late menopause. As it is one of the leading causes of women fatality, it is quite important to detect and classify breast cancer at an early stage [4]. So that proper treatment can be done. It is seen that 90% of patients having breast cancer diagnosed at an early stage are cured [5]. This is one of the reasons which inspire researchers to give a more accurate framework to detect breast cancer. Any abnormality in the breast can be identified with

imaging modality as breasts are superficial organs in the human body. Mammograms and ultrasound are very popularly used image modalities for the early detection of breast cancer. Mammography is a process that uses low-dose X-ray to take the breast image to diagnose breast cancer from different angles of projection [3]. However, ultrasound is a non-radioactive and low-invasive procedure that takes the image from different angles and the pressure of the probe.

Manual diagnosis of disease is a costly, time-consuming as well as an error-prone process. Manual detection of abnormality is difficult as the symptom at an early stage is very small and may not be detected due to oversight. This issue can be overcome by introducing a Computer-aided design (CAD)-based system for automated breast cancer detection to aid radiologists [6,7]. This gives a reliable, fast, and cost-efficient diagnosis.

The development of a CAD system improves the disease diagnosis performance [8–10]. Recently, machine and deep learning-based breast cancer detection are rapidly growing as a preferred approach in the biomedical field. These techniques come up with a more accurate and precise diagnosis of suspicious lesions. Various approaches have been suggested by many researchers for breast cancer detection. In

* Corresponding author.

E-mail addresses: adyashasahu8@gmail.com (A. Sahu), pradeepkumar.das@vit.ac.in, pdas391@gmail.com (P.K. Das), smeher@nitrkl.ac.in (S. Meher).

traditional machine learning approaches, segmentation plays a vital role in boosting the overall performance for classification [3,11,12].

Nonetheless, huge training data is required to achieve better accuracy in deep-learning-based approaches. Usually, medical image datasets are small in size, which yields an appreciable amount of training errors. To overcome this problem, transfer learning (TL) has been widely used in recent years. Here, a pre-trained model is generated by training the model over a large dataset (source domain), then finetuning it on a small dataset (target domain). Hence, in recent times transfer learning has been preferred over traditional deep learning techniques for medical image processing [13,14]. This influences us in developing an efficient automatic CAD system that ensembles three efficient transfer learning techniques to detect breast cancer using mammograms.

The main contributions of the proposed work are mentioned below.

- A new efficient automated breast cancer detection system is proposed by ensembling three efficient transfer learning models: AlexNet, ResNet, and MobileNetV2. It exhibits admirable performance due to the combined benefits of these three techniques. Moreover, the use of transfer learning techniques makes the system computationally more efficient than traditional deep learning approaches.
- The employment of residual learning, depthwise separable convolution, and inverted residual bottleneck structure make the system faster, whereas skip connection makes the optimization of the deep network easier.
- As a preprocessing step prior to the deep ensemble framework, a Laplacian of Gaussian-based modified high boosting filter (LoGMHBF) is used to further improve image quality and performance by combining the benefits of LoG and high boosting filter.

The rest of this paper is organized as follows: Section 2 presents related work. Section 3 explains the proposed deep learning-based breast cancer classification framework for effective breast cancer detection. Here, we have discussed three models, which have been ensembled for breast cancer detection viz. AlexNet, ResNet18, and MobileNetV2. The data used in this work is described briefly in Section 3. In Section 4, we present and discuss the experimental results obtained. Section 4 comprises the significance of the proposed method. In the end, Section 5 concludes the paper with a brief explanation.

2. Related work

Though many researchers have studied deep learning for decades, major advancements in the field of biomedical image processing are achieved recently and have evolved as a fast-growing research area. Several research works have been done on CAD-based systems for automated breast cancer detection. Here, we have compiled the related works employing mammography and ultrasound images with Machine learning and Deep learning systematically and have highlighted their contributions and limitations as shown in Table 1.

In the recent past, several researchers have worked on ensemble learning methods in breast cancer detection for improving classification performance. Abdar et al. [15] have introduced a nested ensemble method for automatic breast cancer detection. Here, Naive Bayes, Bayesian Networks, Stochastic Gradient Descent, and Logistic Model Trees are used as base classifiers. They find that the proposed method (two-layer nested ensemble classifiers) gives better performance than the single classifiers. In 2019, Abdar et al. [16] have suggested an ensemble classifier taking SVM and ANN as the base models and found noticeable classification results. Shakeel et al. [17] have presented an efficient system to detect breast cancer in 2021. They have extracted the crucial features from the region of interest, and then used SVM for classification. In [18], the authors have preprocessed the ultrasound

Table 1
Recent related works on breast cancer detection.

Ref./ Year	Methodology	Limitations
[21] 2017	Present a Hilbert filling space-based feature extraction and ensemble classifier using weighted majority voting.	The selection of ROI (Region of interest) for both normal and abnormal cases should be adaptive for robustness. However, ROI was manually selected.
[5] 2019	Dilated convolution is applied for feature extraction followed by multi-view CNN to classify.	For features extraction, they used a dilated convolution layer having factors 1, 2, and 4. Did not perform feature selection. Comparisons is done only on basis of accuracy.
[22] 2019	Presented a CNN and TL scheme to detect breast cancer.	The system is quite computationally expensive and the proposed preprocessing method may not work for high-resolution images.
[23] 2019	Proposed improved DenseNet structure i.e. DenseNet	The focus of this work is solely on malignancy identification. The performance can yet be enhanced.
[24] 2020	Proposed a modified version of ResNet and InceptionV3	It focuses on malignancy detection. K-fold cross-validation performance was not presented by the authors. The classification performance is significantly less.
[25] 2020	Presented an ensemble classifier on mammograms with low contrast.	Due to the multiplication of matrix values in the CNN model and the extraction of both CNN and RNN-based features, this technique is highly time-consuming.
[26] 2021	Suggested an ensemble feature extraction technique, then a neural network for classification.	This method places more focus just on malignancy detection than it does on both malignancy and abnormality identification. The hold-out approach is used for performance analysis rather than k-fold cross-validation.
[27] 2021	Proposed a TL technique with a deep representation scaling layer	The nonlinear scaling function may achieve better discrimination ability instead of linear scaling there was a possible options for the scaling
[28] 2021	Presented an adaptive spatial feature fusion method	Instead of using conventional ANN for classification any advanced classifier or ensemble classifier may improve the performance. Only malignancy detection is done.
[7] 2022	Suggested a deep CNN model for diagnosis of breast cancer.	This model consists 4 convolution layers and 1 fully connected layer, which yields poor performance. This results from a restricted capacity for learning various feature sets. Additionally, it costs more to compute than certain transfer learning models.

images using intensity inhomogeneity correction and then applied deep learning models for the classification of benign and malignant. In 2021, Maqsood et al. [19] have proposed a transferable texture CNN scheme for efficient breast malignancy detection using mammograms. For classification they have utilized sparse-based feature fusion preceded by different transfer learning-based classification. Zebari et al. [20] have presented a comprehensive review in 2021 on CAD-based breast cancer detection using mammograms during the period 2018 to 2020.

Again in 2021 Zebari et al. [29] have presented a breast lesion identification framework, where they have divided the extracted ROIs into five blocks and applied wavelet-based denoising followed by a modified fractal dimension for feature extraction. ANN is employed for the classification. Meraj et al. [30] have suggested a quantization-based UNet approach in 2021 to detect breast lesions. Deep features extracted from DenseNet are fused with the features from Independent Component Analysis to improve performance.

Though the classification results of some papers are quite encouraging, we understand that there is a vast scope to work further in exploring new ensemble classifiers for effectively classifying mammographic and ultrasonic data with much higher accuracy. In most of the work, classical machine learning techniques are ensembled for the

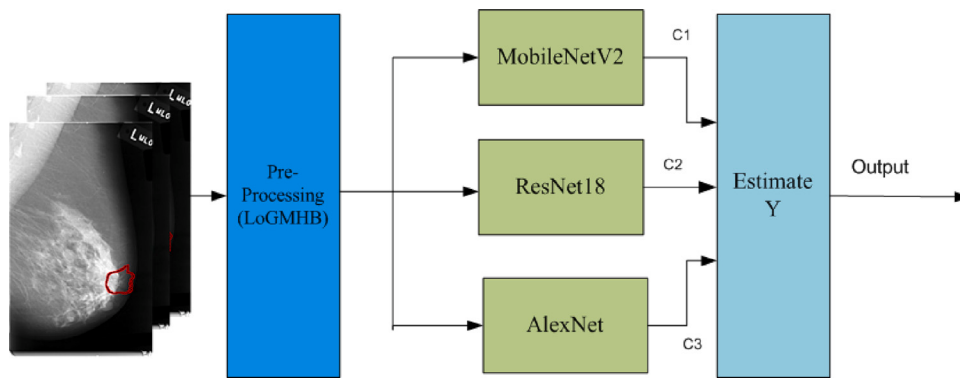


Fig. 1. Schematic diagram of the proposed ensemble technique for breast cancer detection.

detection and classification of breast cancer. However, to achieve better overall performance it is required to improve both the feature extraction and classification performances. In addition most of the works focus only on identification of malignancy rather than identification of both abnormality and malignancy or three class classification of normal, benign, and malignant class. On the other hand, the recent advancements in transfer learning have motivated us to work further in this direction due to its excellent performance in small datasets.

In this work, an efficient automated breast cancer detection system is proposed by ensembling three efficient transfer learning models: AlexNet, ResNet, and MobileNetV2. Usually, a transfer learning model exhibits promising performance even in small datasets since a pre-trained model (trained in the source domain using a large dataset) is only fine-tuned in the target domain. In this work, the proposed model exhibits admirable performance due to the combined benefits of these three techniques. More importantly, the employment of residual learning, depth-wise separable convolution, and inverted residual bottleneck structure makes the system faster, whereas skip connection makes the optimization of the deep network easier. In addition, ReLu is responsible for enhancing nonlinearity, which leads to more accurate classification. In addition, data augmentation is done for proper training and to avoid overfitting. A LoGMHF-based preprocessing is done for denoising, edge enhancement, and deburring to boost the quality of the image. Hence the proposed model exhibits admirable performance even with small datasets.

3. Proposed method

In this section, we propose an efficient ensemble learning-based breast cancer detection and classification system. During last few years, transfer learning algorithms have been widely employed for automatic disease identification because they perform well even with limited amounts of data. Transfer learning addresses the concerns with traditional deep learning networks like performance degradation in small databases due to a lack of data for proper training. It encourages us to offer an effective transfer learning-based breast cancer detection network, as illustrated in Fig. 1, that performs well even in small databases. Here, our objective is to achieve outstanding performance with a computationally efficient system. Hence, we come up with an efficient method, that ensembles three popular transfer learning networks viz. AlexNet, ResNet, and MobileNetV2. This work includes two steps: abnormality detection followed by malignancy detection. Abnormality detection classifies the normal and abnormal breast images; whereas malignancy detection classifies benign and malignant images among abnormal images. Along with this we have also evaluated the three class classification performance directly and classified into normal, benign, and malignant.

3.1. Preprocessing

In general, the quality of medical photographs has degraded due to unwanted sounds and blurring effects, which result in erroneous detection during diagnosis. As a result, image preprocessing is essential to maximize image quality. In this case, a LoG-based modified high-boosting (LoGMHB) operation is carried out before the classification step as pre-processing to obtain a denoised deblurred image [31].

The Laplacian operator deblur the image preserving the edges. At the same time it is vulnerable to noise. This issue is addressed by employing a 2-D Gaussian filter before the Laplacian operator to lessen the influence of noise and it operates as a LoG filter, which is expressed as the following equation.

$$P_m(i, j) = I_m(i, j) + kL_{gf}(i, j) \quad (1)$$

$I(i, j)$ is the input image whereas $P(i, j)$ is the preprocessed output image in Eq. (1). The weight factor k value is chosen in trial basis for which the image quality improve significantly. After performing the LoG operation on the input picture, the expression is as follows:

$$L_{gf}(i, j) = \frac{-1}{\pi\delta^4} \left(1 - \frac{i^2 + j^2}{2\delta^2} \right) \exp \left(-\frac{i^2 + j^2}{2\delta^2} \right). \quad (2)$$

Here, choosing a correct value of standard deviation (σ) and k value plays a vital role to improve the image quality. In this work, $k = 1.5$, $\sigma = 1$, and LoG filter kernel size is 7×7 .

3.2. CNN architecture

In the ensemble technique, we create multiple models which work together on a common dataset and then combine them that yield better results. The principle of ensemble learning is combine weak learners together to give a strong learner and thus results in increased performance. Usually, this method gives a better prediction than each of the base methods. Majority voting is a type of ensemble learning where the output of each base classifier is combined and the final result is predicted by the majority of votes to a single class by base classifiers. It is the least biased result of the particular base classifier as the majority number of votes are counted.

Suppose the class predicted by majority voting is labeled as Y . Each classifier voting is $C_k(x)$.

$$Y = \text{mode} \{C_1, C_2, \dots, C_k\} \quad (3)$$

3.3. AlexNet

In 2012, Krizhevsky et al. have proposed AlexNet [32], a well-known transfer learning approach utilized in several applications of computer vision. As shown in Fig. 2 the structure of this network contains 8 weighted layers: five convolution layers followed by three fully-connected layers. Images of size $227 \times 227 \times 3$ are fed to the network,

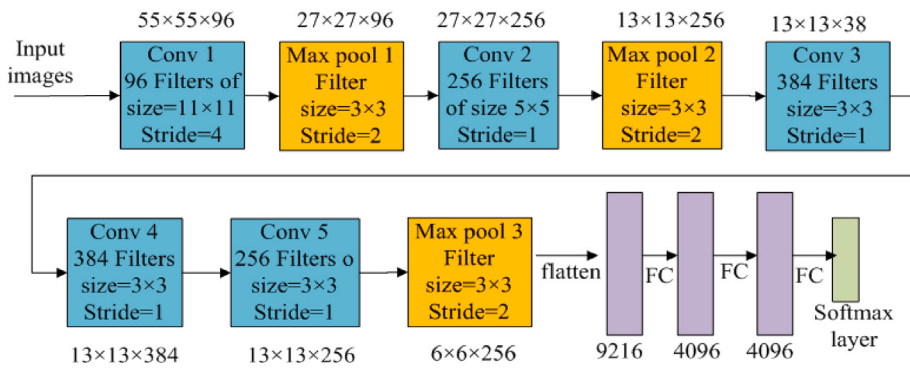


Fig. 2. Architecture of AlexNet [32].

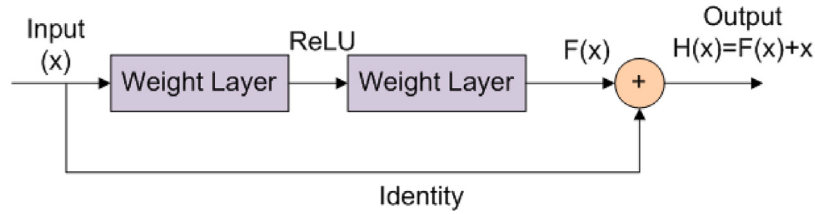


Fig. 3. Skip connection.

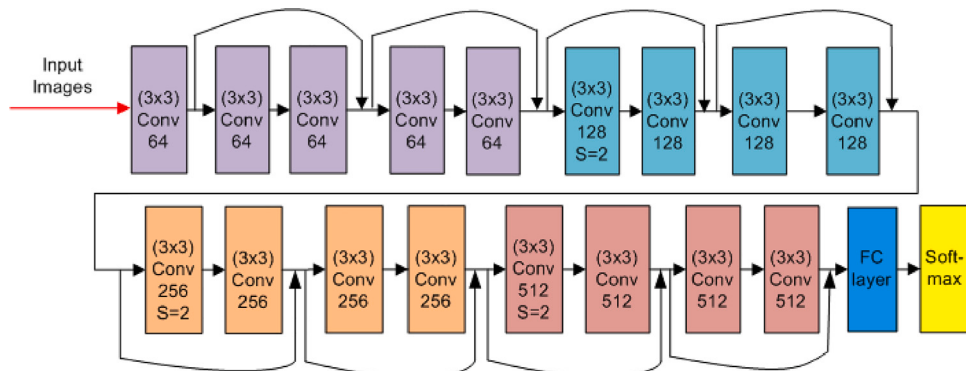


Fig. 4. ResNet 18 model for breast cancer detection [33].

initially. The first convolutional layer uses 96 kernels of size 11×11 with stride 4. The second one has 256 kernels of size 5×5 . After each convolution layer, there is a max-pooling layer. The third convolutional layer contains 384 kernels of size 3×3 and fourth third convolutional layer consists 384 kernels of size 3×3 . The fifth convolutional layer (256 kernels of size 3×3) is connected directly without any pooling layers and continued by a Max-Pooling layer, which is attached with a series of two fully connected layers. Each of the fully connected layers has 4690 neurons. Finally, there is a softmax layer having 1000 labels of class. Here ReLU activation function is used, which makes the network faster. Dropout is employed to deal with overfitting.

3.4. ResNet

He et al. have introduced ResNet [33] in 2015. Its depth can be up to 152 layers, which made it more popular. Usually, more number layers result in better separability and hence increased classification performance. However, it is found that the accuracy gets saturated and then starts degrading after a certain number of layers in the network, due to the vanishing gradient problem. To solve this issue, ResNet came up with the concept of skip connection or identity mapping, as presented in Fig. 3. It is just a type of replication that allows copy the

input to the next layer by giving an substitute pathway for gradient flow [33]. The network architecture of ResNet18 is presented in Fig. 4.

In the above figure, we can see that input of the first layer is replicated to the second layer output. By the using of residual identity mapping, the high-resolution feature maps of the shallower layers are directly added to the lower-resolution maps from the deeper layers in Residual networks.

3.5. MobileNetV2

MobileNetV2 [34] is an effective transfer learning technique for its inverted residual structure which is having a shortcut connection between two thin bottleneck layers. Lightweight depthwise separable convolution is another important feature of MobileNetV2. The architecture of MobileNetV2 contains 17 bottleneck layers and 3 convolution layers are shown in Fig. 5. The detailed information on the each layer is also given. ReLU6 is used to add non-linearity because it is robust when used with low-precision computation. Some important features of MobileNetV2 are described as follows.

3.5.1. Depthwise separable convolutions

General convolution is a process where simultaneous filtering occurs over all the input channels in conjunction with the summation of all these values.

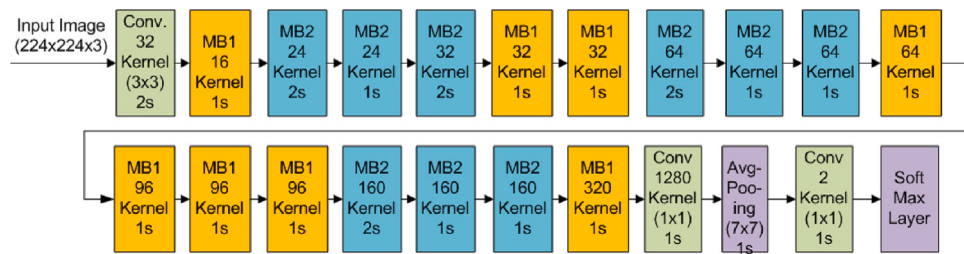


Fig. 5. MobileNetV2 model for breast cancer detection [34].

In the general convolution process, we apply a filter over all the input channels simultaneously and then combine all the values to get the output. In MobileNetV2, to make the network faster Depthwise separable convolutions are used instead of the computationally expensive general convolution operation. Depthwise separable convolution is carried out in two steps: depthwise convolution and pointwise convolution. In depthwise convolution, we execute convolution on a single input channel simultaneously. However, pointwise convolution is 1×1 convolution, which is the linear combination of each output layer in depthwise convolution.

In a normal or classical convolution, k kernels of size $D_f \times D_f \times 1$ are applied on the input of size $D_t \times D_t \times p$ to generate the output of size $D_g \times D_g \times p$. Hence the computational cost of a normal convolution is

$$C_{gen} = D_f^2 \times D_g^2 \times k \times p. \quad (4)$$

Depthwise convolutions

Here the filter of size $D_f \times D_f \times 1$ is applied on the same input of size $D_t \times D_t \times p$. Number of multiplication for a single kernel is D_f^2 and hence the total number of multiplication for a kernel over the input image is $D_f^2 \times D_g^2$.

The input image contains p channels. So p number of kernels are required for p number of channels. Therefore the total number of multiplication needed in depthwise convolutions is

$$M_{dc} = D_f^2 \times D_g^2 \times p \quad (5)$$

Pointwise convolutions

Here, a kernel of size $1 \times 1 \times p$ is applied to combine each output of shape $D_g^2 \times p$ of depthwise convolution. So the number of multiplication needed is $D_g^2 \times p$. For f number of kernels, the number of multiplication needed is expressed as:

$$M_{pc} = D_g^2 \times p \times f \quad (6)$$

The total number of multiplication required in depth-wise separable convolution is

$$M_{ds} = M_{dc} + M_{pc}. \quad (7)$$

From Eqs. (4) and (7), Eq. (8) may be rewritten as:

$$M_{ds} = D_f^2 \times D_g^2 \times p + D_g^2 \times p \times f. \quad (8)$$

By comparing Eqs. (1) and (7), the relative computational complexity of depthwise separable convolution over general convolution λ , is given by:

$$\lambda = \frac{M_{ds}}{M_{gen}} = \frac{D_g^2 \times p(D_f^2 + f)}{D_f^2 \times D_g^2 \times p \times f} = \frac{1}{D_f^2} + \frac{1}{f}. \quad (9)$$

Here, for a 3×3 kernel and for an image of size $224 \times 224 \times 3$ pixels, the factor

$$\lambda = \frac{1}{3^2} + \frac{1}{75 \times 75} \approx \frac{1}{9} \quad (10)$$

The minimum number of 3×3 kernels required to filter an image of size $224 \times 224 \times 3$ is 76, where at least each pixel is used for filtering

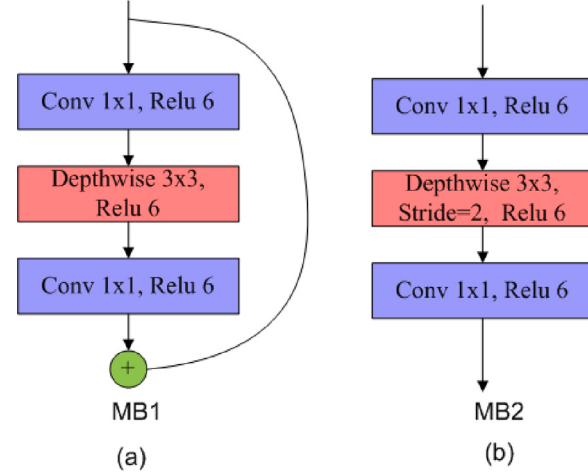


Fig. 6. Basic blocks used in MobileNetV2 architecture: (a) block having stride 1, (b) block having stride 2 [34].

at once. More importantly, the factor 1 is almost 9 even the number of filters increases. This implies that the depthwise separable convolution is almost 9 times faster in computational complexity than a general convolution. Hence it is preferred for fast training and fast execution.

3.5.2. Inverted residuals

Like residual block, inverted residual block improves the capability for gradient flow by providing an alternate path for gradient flow. However, the short connections are implemented directly between the bottlenecks, unlike residual blocks. In order to make the network more efficient, 2 types of standard bottleneck structures: MobileNetV2 block-1 (MB1) and MobileNetV2 block-2 (MB2) are employed in MobileNetV2 as shown in Fig. 6. Fig. 6(a) shows an inverted residual bottleneck structure with stride = 1 (MB1), whereas Fig. 6(b) shows the bottleneck structure with stride = 1 or 2 (MB2).

3.5.3. Linear bottlenecks

To optimize the network, a low-dimensional manifold of interest should be maintained. This can be achieved by employing a linear bottleneck structure. Bottleneck structure is a 1×1 convolution which is introduced before an expensive convolution (e.g. 3×3 or 5×5). It reduces the depth keeping the size the same as before to get a computationally more efficient network. To minimize the information loss the bottleneck layer is linear in MobileNetV2.

4. Datasets

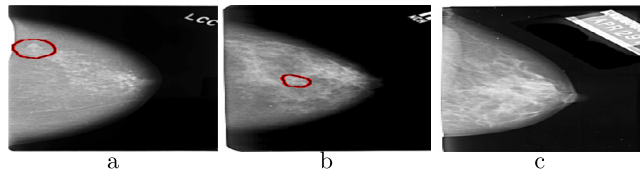
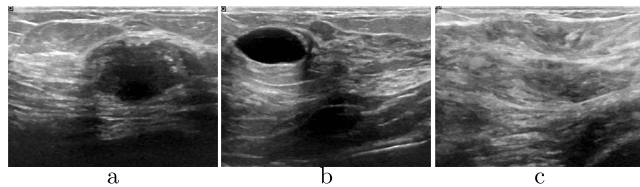
For experimentation, the proposed method, as well as the comparing methods, are implemented over three popular publicly available datasets: mini-DDSM dataset for mammograms and the BUSI and BUS2 datasets for ultrasound images. The mini-DDSM [35] dataset total 9684 X-ray images from 2620 cases in 16-bit format. Each case has

Table 2

Distribution of images for training and testing.

Dataset	Total sample				Training sample				Testing sample			
	Abnormality		Malignancy		Abnormality		Malignancy		Abnormality		Malignancy	
	A	N	M	B	A	N	M	B	A	N	M	B
DDSM	400	200	200	200	360	180	180	180	40	20	20	20
BUSI	260	130	130	130	234	117	117	117	26	13	13	13
BUS2	-	-	100	100	-	-	90	90	-	-	10	10

A- Abnormal images; N- Normal images; B- Benign images; M- Malignant images.

**Fig. 7.** Breast mammograms taken from mini-DDSM [35]: (a) Malignant, (b) Benign and (c) Normal.**Fig. 8.** Breast ultrasounds from BUSI [36]: (a) Malignant, (b) Benign and (c) Normal.

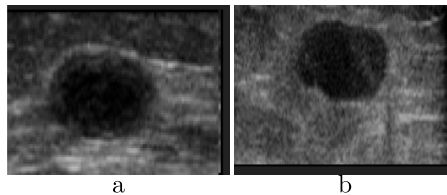
mediolateral oblique (MLO) and craniocaudal (CC) views of the left and right breast, for the MLO view image is captured at an angle of 30 degrees or 60 degrees, whereas the CC view is taken from above. Similarly, the BUSI [36] contains 780 images, of which 437 are benign, 210 are malignant, and 133 are normal, whereas BUS2 [37] consists a total of 250 ultrasonic images, out of which 150 are non-cancerous and 100 are malignant or cancerous. All three datasets include the ground truth information given by the experts, whether it is benign or malignant or normal breast image. In this work, to validate the performance of the proposed scheme with small data, we have taken a subset of 600 mammograms from the mini-DDSM dataset. This subset contains 200 normal, 200 benign, and 200 malignant mammogram images. In the same way, from the BUSI dataset, a subset containing 130 normal, 130 benign, and 130 malignant images is extracted to carry out the experiment. A set of 200 images (100 malignant and 100 benign) is utilized in this work from the BUS2 dataset. The number of images used for training and testing to identify of abnormality and malignancy are shown in Table 2. Since we are doing 10-fold-cross validation for performance evaluation, in each fold, 90% of images are used for training, and the rest 10% of images are used for testing. The table shows the number of training and testing samples out of the total number of samples used of training and testing for all three datasets. Figs. 7–9 show the breast images of classes: malignant, benign, and normal taken from mini-DDSM, BUSI, and BUS2 datasets, respectively.

In Table 2, the symbols denote as follows.

A- Abnormal images; N- Normal images; B- Benign images; M- Malignant images

5. Results and discussion

In this section, we have presented a comparative performance analysis for breast cancer detection. To make the performance analysis fairer, we have done 10-fold cross-validation for comparative performance analysis instead of showing the performance of a single observation. The performance of the proposed method is compared

**Fig. 9.** Breast ultrasounds from BUS2 [37]: (a) Benign, (b) Malignant.

with some other popular transfer learning-based breast classification methods (e.g., Vgg19, AlexNet, Xception, ResNet18, MobileNetV2, InceptionV3, and NasNetmobile) as well as other combinations of ensemble classifiers using the mini-DDSM (mammogram), BUSI and BUS2 dataset(ultrasound). We have tried all the possible combinations using these base classifiers and presented four well-performing combinations of ensemble classifiers as presented below.

Ensemble1 (E1) = MobileNetV2+VGG19+AlexNet

Ensemble2 (E2) = MobileNetV2+Xception+ResNet18

Ensemble3 (E3) = MobileNetV2+Xception+AlexNet

Proposed (E4) = MobileNetV2+ResNet18+AlexNet

To quantify the performance of all the above-mentioned methods, six popular standard performance measures are used, viz. AUC, specificity, accuracy, F1 score, sensitivity, and precision. The whole experimental work is implemented using a system having Intel Xeon Core i7 processor, 3.50 GHz clock speed, NVIDIA GeForce RTX A4000 16 GB GPU, and 64 GB RAM with MATLAB R2020b. Here, the maximum number of epochs taken is 60, the learning rate (controls the training speed) is 0.0001, and the minimum batch size is 64. We have executed all the methods on this platform for a fair and genuine comparison.

In ensemble network, we train the base classifiers during training stage, where as in testing stage the prediction is done based upon the corresponding class predicted by the base classifiers. Hence, the accuracy and loss graph of the three base classifiers: AlexNet, ResNet18, and MobileNetV2 involved in the proposed ensemble framework is presented in Figs. 10 through 16. For mini-DDSM dataset the accuracy and loss graphs for AlexNet, ResNet18, and MobileNetV2 are presented in Figs. 10, 11, and 12, respectively to detect abnormality and malignancy. Similarly, Figs. 13–15 shows the accuracy and loss graphs for abnormality and malignancy detection, for the base classifiers: AlexNet, ResNet18, and MobileNetV2, respectively on BUSI dataset. Fig. 16 depicts the loss graph for AlexNet and ResNet18, whereas Fig. 17 shows the loss graph for MobileNetV2 on BUS2 dataset.

Table 3 depicts the performance comparison of the suggested ensemble classifier with other transfer learning techniques to detect abnormality using the mini-DDSM dataset. From this table, we notice that the proposed ensemble classifier beats others with the highest value of quantitative measures (99.75% precision, 99.17% accuracy, 99.00% sensitivity, 99.50% specificity, 0.9937 F1 scores, and 0.9925 AUC). Similarly, the malignancy identification performance comparison in the mini-DDSM dataset is presented in Table 4. From the table, we see the proposed method performing better than the others with 97.99% precision, 97.75% accuracy, 97.50% sensitivity, 98.00% specificity, 0.9774 F1 scores, and 0.9775 AUC.

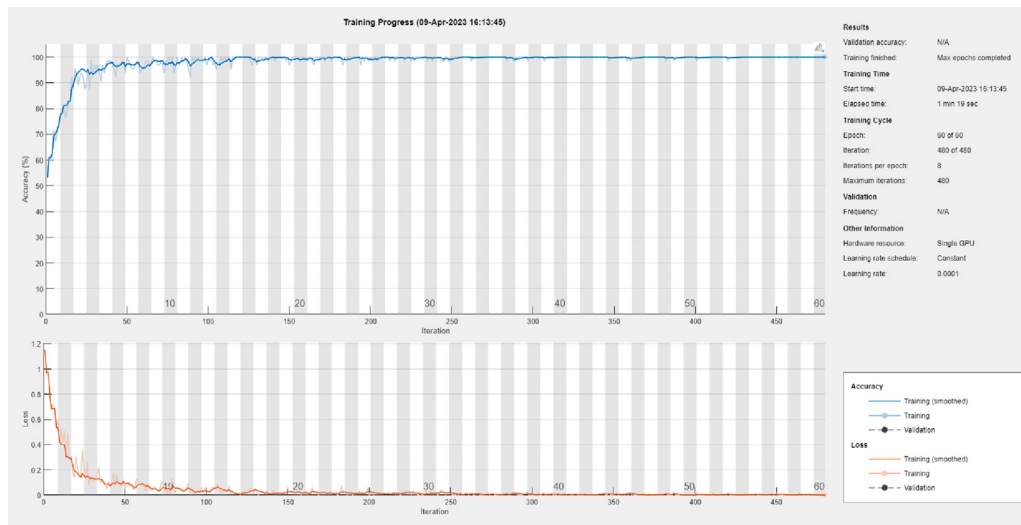


Fig. 10. Accuracy and loss graph for AlexNet for abnormality identification on mini-DDSM dataset.

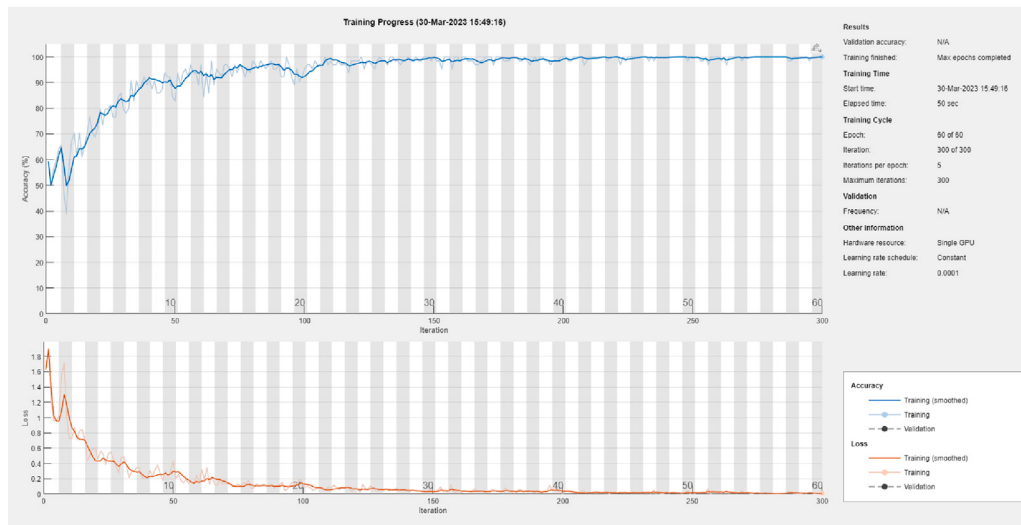


Fig. 11. Accuracy and loss graph for AlexNet for malignancy identification on mini-DDSM dataset.

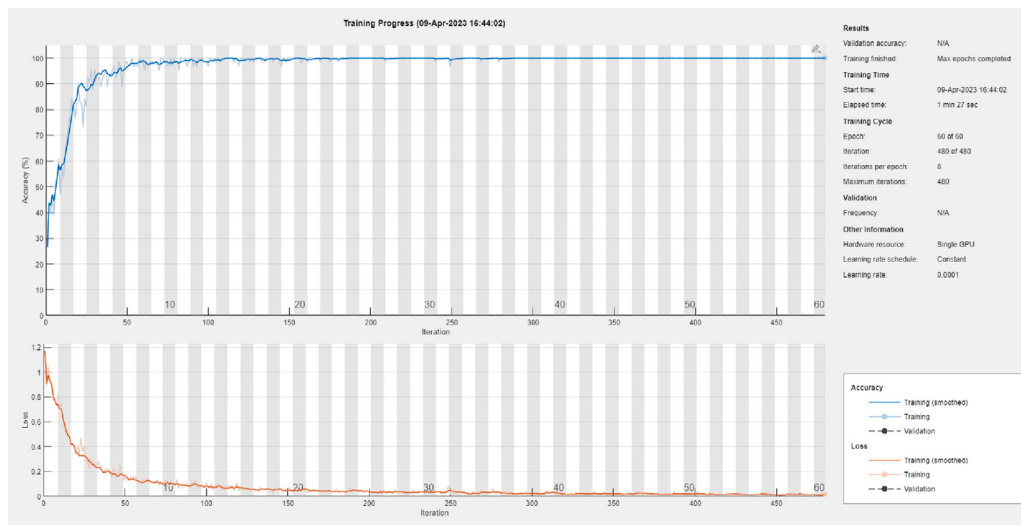


Fig. 12. Accuracy and loss graph for ResNet18 for abnormality identification on mini-DDSM dataset.

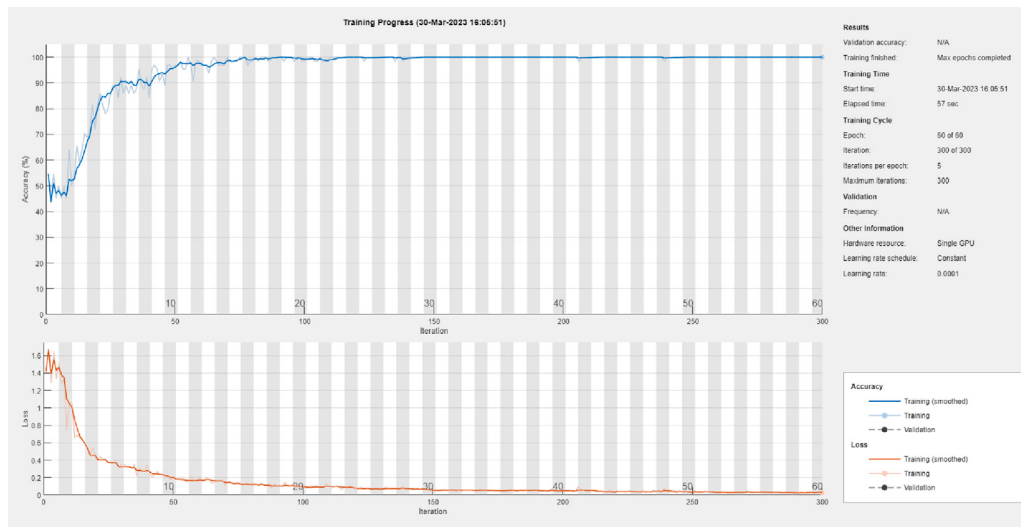


Fig. 13. Accuracy and loss graph for ResNet18 for malignancy identification on mini-DDSM dataset.

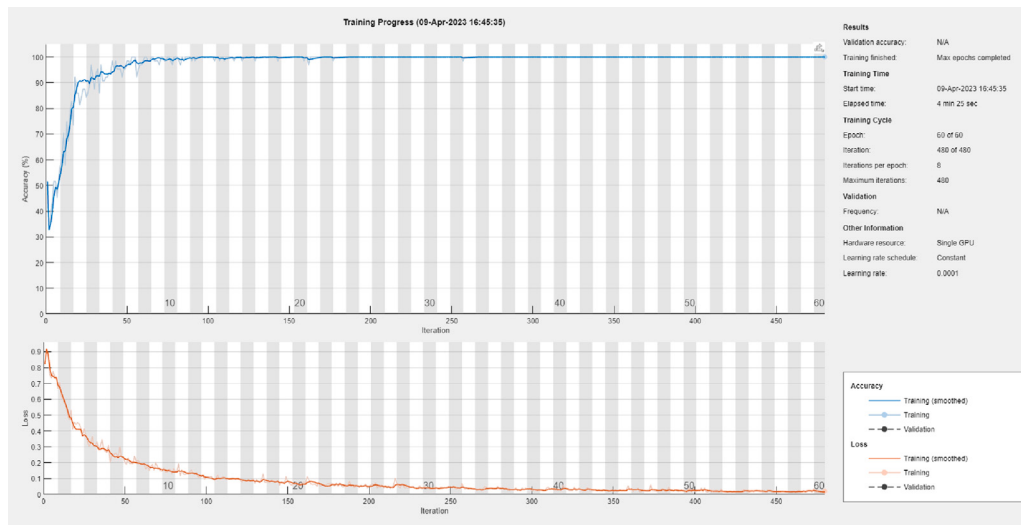


Fig. 14. Accuracy and loss graph for MobileNetV2 for abnormality identification on mini-DDSM dataset.

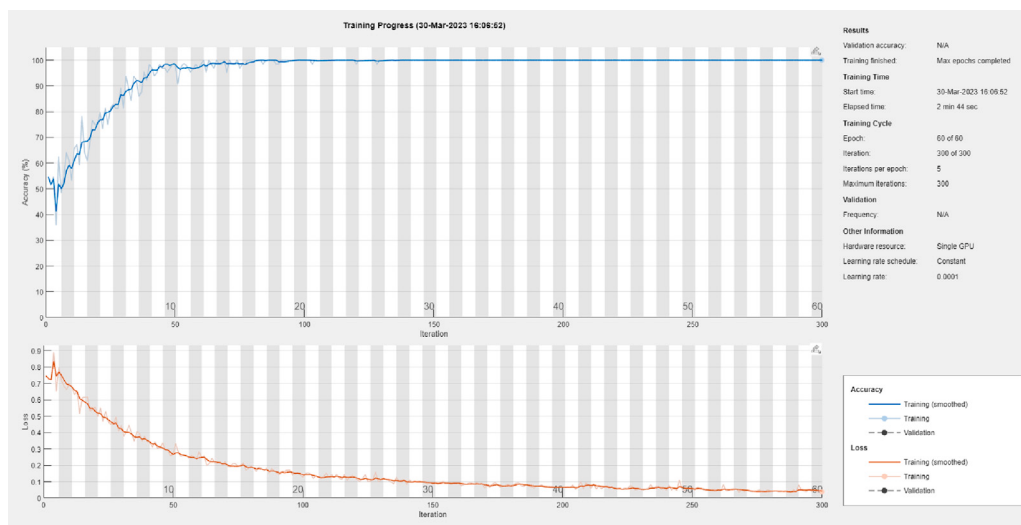


Fig. 15. Accuracy and loss graph for MobileNetV2 for malignancy identification on mini-DDSM dataset.

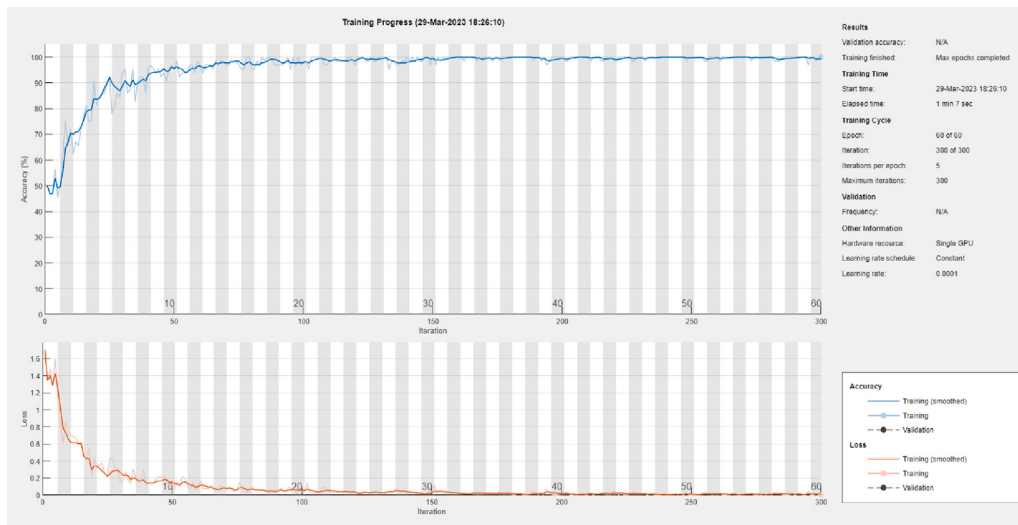


Fig. 16. Accuracy and loss graph for AlexNet for abnormality identification on BUSI dataset.

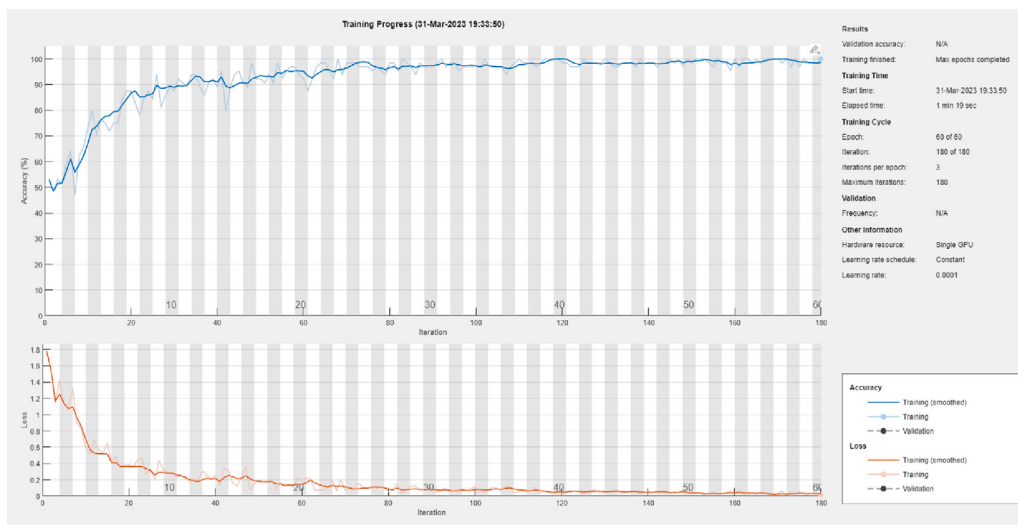


Fig. 17. Accuracy and loss graph for AlexNet for malignancy identification on BUSI dataset.

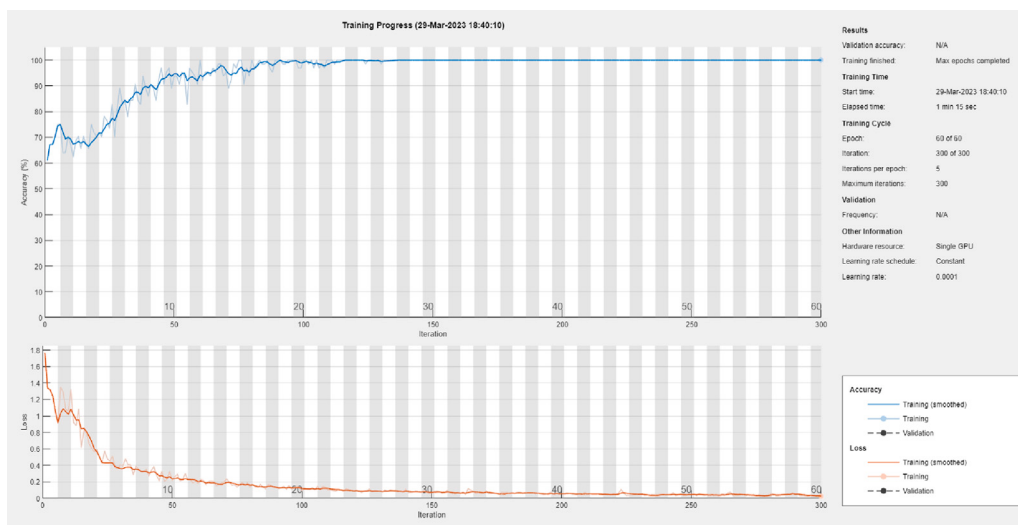


Fig. 18. Accuracy and loss graph for ResNet18 for abnormality identification on BUSI dataset.

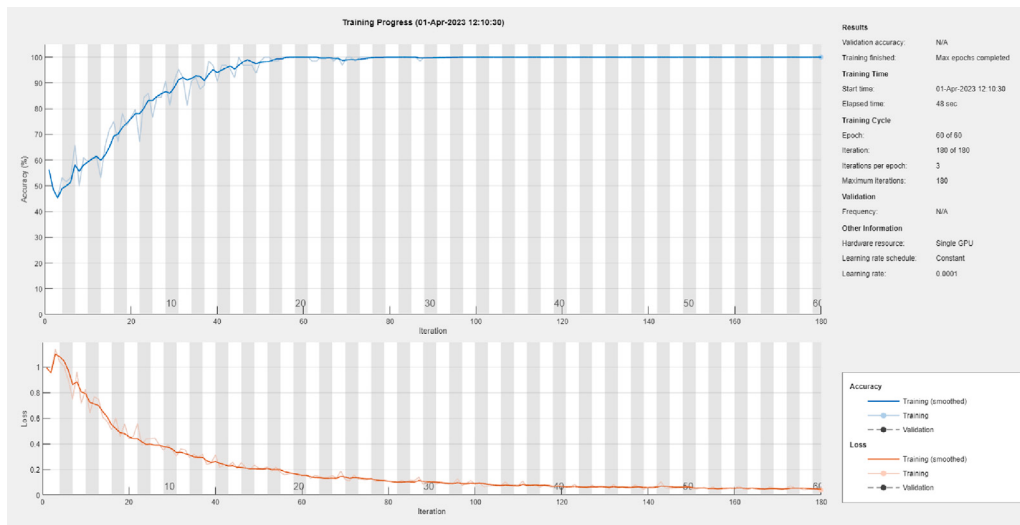


Fig. 19. Accuracy and loss graph for ResNet18 for malignancy identification on BUSI dataset.

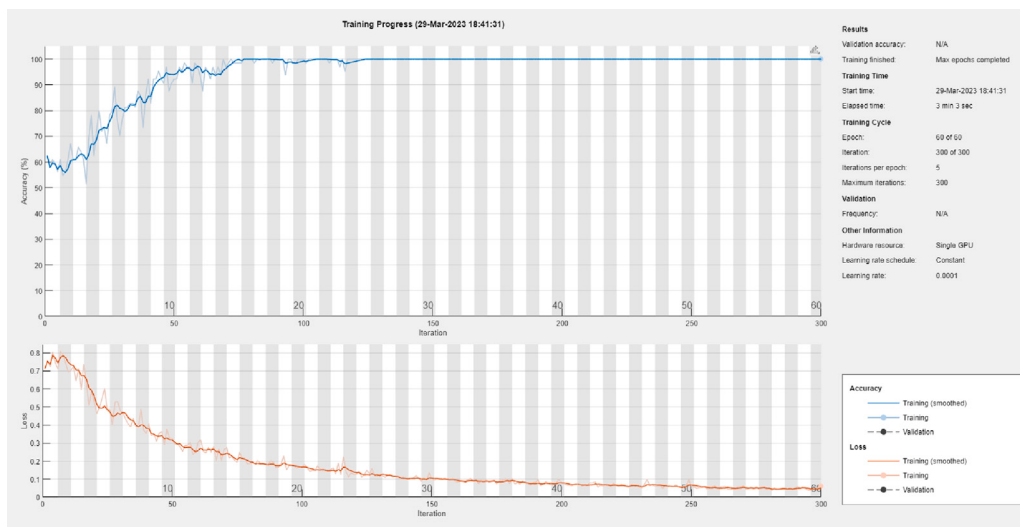


Fig. 20. Accuracy and loss graph for MobileNetV2 for abnormality identification on BUSI dataset.

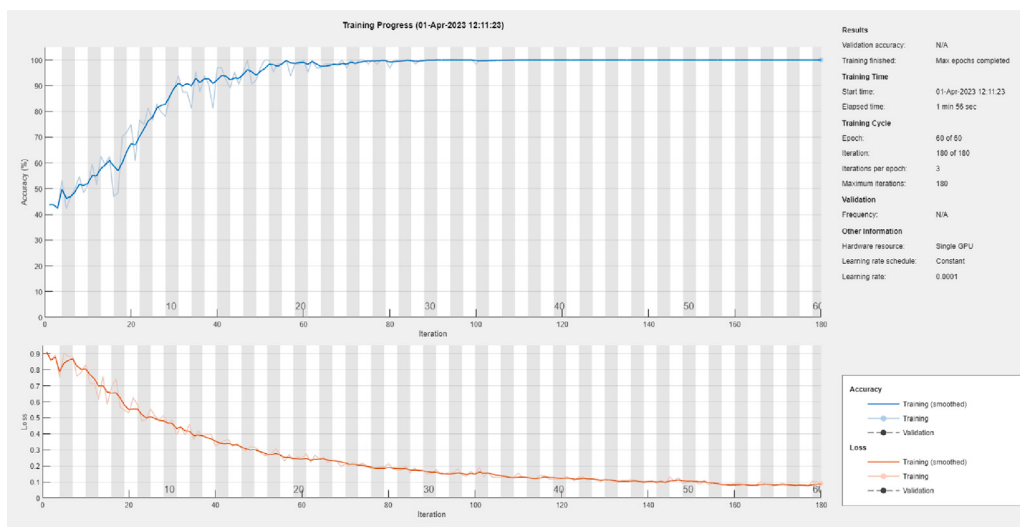


Fig. 21. Accuracy and loss graph for MobileNetV2 for malignancy identification on BUSI dataset.

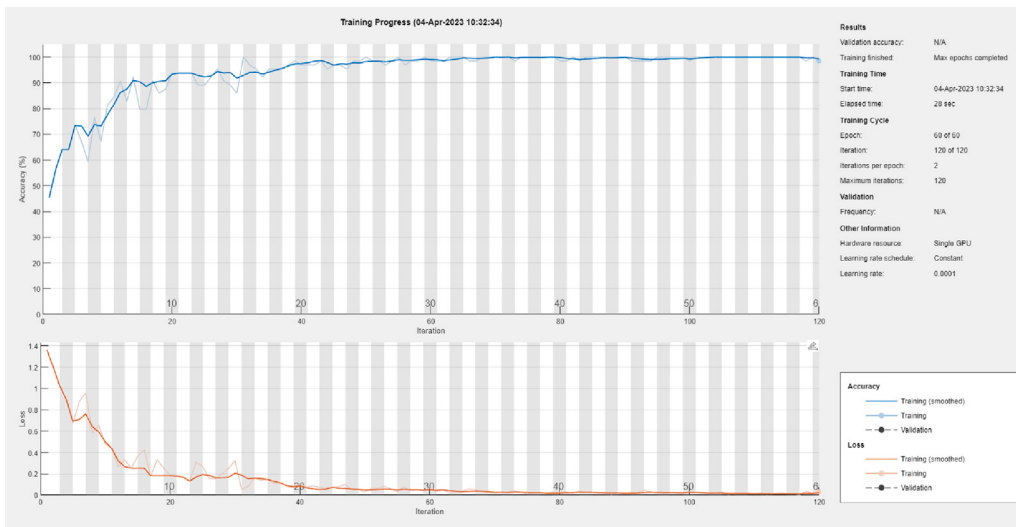


Fig. 22. Accuracy and loss graph for AlexNet on BUS2 dataset for malignancy identification.

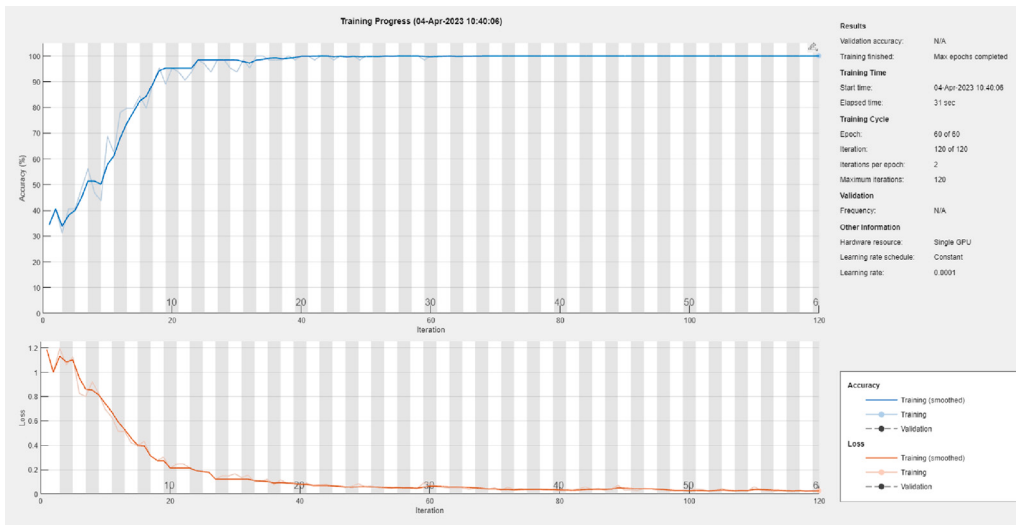


Fig. 23. Accuracy and loss graph for ResNet18 on BUS2 dataset for malignancy identification.

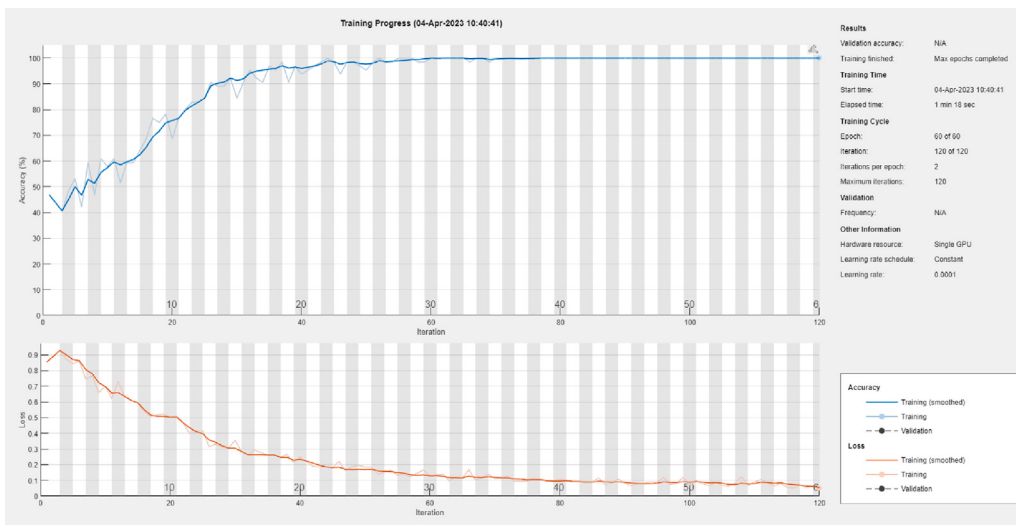


Fig. 24. Accuracy and loss graph MobileNetV2 on BUS2 dataset for malignancy identification.

Table 3
Performance comparison for abnormality detection in mini-DDSM.

Method	AUC	F1 Score	Sensitivity (%)	Precision	Specificity (%)	Accuracy
Vgg19	0.9700	0.9826	98.75	97.77	95.50	97.67
AlexNet	0.9813	0.9862	98.25	98.99	98.00	98.17
Xception	0.8988	0.9470	98.25	91.40	81.50	92.67
ResNet18	0.985	0.9900	98.75	99.25	98.50	98.67
MobileNetV2	0.9875	0.9899	98.50	99.49	99.00	98.67
InceptionV3	0.965	0.9789	98.5	97.28	94.50	97.17
NasNetMobile	0.9638	0.9763	97.75	97.51	95.00	96.83
E1	0.9863	0.9900	98.75	99.25	98.50	98.67
E2	0.9875	0.9912	99.00	99.25	98.50	98.83
E3	0.9850	0.9887	98.50	99.24	98.50	98.50
Proposed	0.9925	0.9937	99.00	99.75	99.50	99.17

Table 4
Performance comparison for malignancy detection in mini-DDSM dataset.

Method	AUC	F1 Score	Sensitivity (%)	Precision (%)	Specificity (%)	Accuracy (%)
Vgg19	0.9375	0.9376	94.00	93.53	93.50	93.75
AlexNet	0.9450	0.9458	96.00	93.20	93.00	94.50
Xception	0.7950	0.7808	73.00	83.91	86.00	79.50
ResNet18	0.9650	0.9650	96.50	96.50	96.50	96.50
MobileNetV2	0.9575	0.9572	95.00	96.45	96.50	95.75
InceptionV3	0.9300	0.9303	93.50	92.57	92.50	93.00
NasNetMobile	0.9300	0.9303	93.50	92.57	92.50	93.00
E1	0.9675	0.9676	97.00	96.52	96.50	96.75
E2	0.9575	0.9473	94.50	94.97	95.00	94.75
E3	0.9425	0.9473	94.50	94.97	95.00	94.75
Proposed	0.9775	0.9774	97.50	97.99	98.00	97.75

Table 5
Performance comparison for abnormality detection in BUSI dataset.

Method	AUC	F1 Score	Sensitivity (%)	Precision (%)	Specificity (%)	Accuracy (%)
Vgg19	0.8731	0.9245	94.23	90.74	80.77	89.74
AlexNet	0.9404	0.9573	95.00	96.48	93.08	94.36
Xception	0.6481	0.8492	99.62	74.00	30.00	76.41
ResNet18	0.8815	0.9286	95.00	90.81	80.77	90.26
MobileNetV2	0.9231	0.9502	95.38	94.66	89.23	93.33
InceptionV3	0.8481	0.9172	95.77	87.99	73.85	88.46
NasNetMobile	0.8192	0.8850	87.31	89.72	80.00	84.87
E1	0.9327	0.9580	96.54	95.08	90.00	94.36
E2	0.8654	0.9304	97.69	88.81	75.38	90.26
E3	0.9173	0.9551	98.08	93.07	85.38	93.85
Proposed	0.9635	0.9770	98.08	97.33	94.62	96.92

Table 6
Performance comparison for malignancy detection in BUSI dataset.

Method	AUC	F1 Score	Sensitivity (%)	Precision (%)	Specificity (%)	Accuracy (%)
Vgg19	0.8654	0.8718	91.54	83.22	81.54	86.54
AlexNet	0.9077	0.9117	95.38	87.32	86.15	90.77
Xception	0.6692	0.6742	68.46	66.42	65.38	66.92
ResNet18	0.9115	0.9126	92.31	90.23	90.00	91.15
MobileNetV2	0.9154	0.9179	94.62	89.13	88.46	91.54
InceptionV3	0.7808	0.7927	83.85	75.17	72.31	78.08
NasNetMobile	0.8116	0.8078	79.23	82.4	83.08	81.15
E1	0.9154	0.9179	94.62	89.13	88.46	91.54
E2	0.8926	0.8963	93.08	86.43	85.38	89.23
E3	0.8731	0.8800	93.08	83.45	81.54	87.31
Proposed	0.9461	0.9465	95.38	93.94	93.85	94.62

The experimental results for the ultrasound dataset (BUSI) are shown in [Tables 5](#) and [6](#) to detect abnormality and malignancy, correspondingly. It is seen that the suggested scheme is better than others with 97.33% precision, 96.92% accuracy, 98.08% sensitivity, 94.62% specificity, 0.9770 F1 scores, and 0.9635 AUC to identify an abnormality, and 93.94% precision, 94.62% accuracy, 95.38% sensitivity, 0.9465 F1 scores, 93.85% specificity, and 0.9461 AUC for malignancy identification. [Table 7](#) shows the classification performance to classify

benign and malignant on BUS2 dataset. The comparison table say that the proposed scheme performs well with 97.98% precision, 97.50% accuracy, 97.00% sensitivity, 98.00% specificity, 0.9749 F1 scores, and 0.9750 AUC. To make the analysis better, the confusion matrix to detect abnormality identification and malignancy using the mini-DDSM dataset is given in [Fig. 18](#). In addition, for ultrasound images, the confusion matrix is mentioned in [Fig. 19](#) to detect abnormality and malignancy, respectively, using BUSI dataset. The confusion matrix

Table 7

Performance comparison for malignancy detection in BUS2 dataset.

Method	AUC	F1 Score	Sensitivity (%)	Specificity (%)	Precision (%)	Accuracy (%)
Vgg19	0.9	0.899	89.00	91.00	90.82	90.00
AlexNet	0.9200	0.5789	55.00	93.00	61.11	86.67
Xception	0.8400	0.8351	81.00	87.00	86.17	84.00
ResNet18	0.9400	0.9394	93.00	95.00	94.90	94.00
MobileNetV2	0.9450	0.9436	92.00	97.00	96.84	94.50
InceptionV3	0.9150	0.9154	92.00	91.00	91.09	91.50
NasNetMobile	0.9050	0.9073	93.00	88.00	88.57	90.50
E1	0.9550	0.9548	95.00	96.00	95.96	95.50
E2	0.9400	0.9394	93.00	95.00	94.90	94.00
E3	0.9250	0.9238	91.00	94.00	93.81	92.50
Proposed	0.9750	0.9749	97.00	98.00	97.98	97.50

Table 8

Detection of normal in mini-DDSM dataset.

Method	F1 Score	Recall (%)	Precision (%)	Specificity (%)	Accuracy (%)
Vgg19	0.9596	95.00	96.94	98.50	97.33
AlexNet	0.9727	98.00	96.55	98.25	98.17
Xception	0.8726	80.50	95.27	98.00	92.17
ResNet18	0.9774	97.50	97.99	99.00	98.50
MobileNetV2	0.9776	98.50	97.04	98.50	98.50
InceptionV3	0.9516	93.50	96.89	98.50	96.83
NasNetMobile	0.9471	94.00	95.43	97.75	96.50
E1	0.9775	98.00	97.51	98.75	98.50
E2	0.9800	98.00	98.00	99.00	98.67
E3	0.9751	98.00	97.03	98.50	98.33
Proposed	0.9851	99.00	98.02	99.00	99.00

Table 9

Detection of benign in mini-DDSM dataset.

Method	F1 Score	Sensitivity (%)	Precision (%)	Specificity (%)	Accuracy (%)
Vgg19	0.8889	86.00	91.98	96.25	92.83
AlexNet	0.9016	87.00	93.55	97.00	93.67
Xception	0.6649	62.00	71.68	87.75	79.17
ResNet18	0.9262	91.00	94.30	97.25	95.17
MobileNetV2	0.9238	94.00	90.82	95.25	94.83
InceptionV3	0.8808	90.50	85.78	92.50	91.83
NasNetMobile	0.855	87.00	84.06	91.75	90.17
E1	0.9364	92.00	95.34	97.75	95.83
E2	0.9086	89.50	92.27	96.25	94.00
E3	0.9045	90.00	90.91	95.50	93.67
Proposed	0.9519	94.00	96.41	98.25	96.83

Table 10

Detection of malignant in mini-DDSM dataset.

Method	F1 Score	Sensitivity (%)	Precision (%)	Specificity (%)	Accuracy (%)
Vgg19	0.9042	92.00	88.89	94.25	93.50
AlexNet	0.9165	96.00	87.67	93.25	94.17
Xception	0.7103	76.00	66.67	81.00	79.33
ResNet18	0.9505	96.00	94.12	97.00	96.67
MobileNetV2	0.9344	92.50	94.39	97.25	95.67
InceptionV3	0.8889	88.00	89.8	95.00	92.67
NasNetMobile	0.8872	88.50	88.94	94.50	92.50
E1	0.9423	94.00	94.47	97.25	96.17
E2	0.9189	93.50	90.34	95.00	94.50
E3	0.9169	91.00	92.39	96.25	94.50
Proposed	0.9628	97.00	95.57	97.75	97.50

for malignancy identification in BUS2 is shown in Fig. 20. For better analysis we have also presented the ROC curves. Figs. 21 and 22 show the ROC curve of 6th fold on the mini-DDSM dataset for abnormality and malignancy identification. Similarly Figs. 23 and 24 depicts the ROC curve on BUSI dataset to identify abnormality and malignancy, correspondingly. On the other hand the ROC curve on BUS2 dataset is presented in Fig. 25. As only two classes are present in BUS2

dataset(benign and malignant), only malignancy identification is done in BUS2 dataset (see Figs. 26–32).

Tables 8 to 10 shows the three class classification performance of each class of normal, benign, and malignant in mini-DDSM dataset. Similarly, in BUSI dataset the each class performance i.e. normal, benign, and malignant is presented in Tables 11 to 13, correspondingly. Since BUS2 dataset consists of two classes, three class classification

Table 11
Detection of normal in BUSI dataset.

Method	Precision (%)	Accuracy (%)	Sensitivity (%)	Specificity (%)	F1 Score
Vgg19	88.89	90.00	80.00	95.00	0.8421
AlexNet	91.54	94.36	91.54	95.77	0.9154
Xception	93.18	76.41	31.54	98.85	0.4713
ResNet18	89.83	90.77	81.54	95.38	0.8548
MobileNetV2	91.27	93.33	88.46	95.77	0.8984
InceptionV3	88.68	87.69	72.31	95.38	0.7966
NasNetMobile	76.69	84.87	78.46	88.08	0.7756
E1	92.06	93.85	89.23	96.15	0.9062
E2	93.40	90.26	76.15	97.31	0.839
E3	94.96	94.10	86.92	97.69	0.9076
Proposed	95.38	96.92	95.38	97.69	0.9538

Table 12
Detection of benign in BUSI dataset.

Method	F1 Score	Sensitivity (%)	Precision (%)	Specificity (%)	Accuracy (%)
Vgg19	0.7765	76.15	79.20	90.00	85.38
AlexNet	0.8240	79.23	85.83	93.46	88.72
Xception	0.4616	43.85	48.72	76.92	65.90
ResNet18	0.8538	85.38	85.38	92.69	90.26
MobileNetV2	0.8594	84.62	87.3	93.85	90.77
InceptionV3	0.6561	63.85	67.48	84.62	77.69
NasNetMobile	0.6825	66.15	70.49	86.15	79.49
E1	0.8314	81.54	84.80	92.69	88.97
E2	0.8207	79.23	85.12	93.08	88.46
E3	0.7953	77.69	81.45	91.15	86.67
Proposed	0.9035	90.00	90.70	95.38	93.59

Table 13
Detection of malignant in BUSI dataset.

Method	F1 Score	Sensitivity (%)	Precision (%)	Specificity (%)	Accuracy (%)
Vgg19	0.8015	82.31	78.10	88.46	86.41
AlexNet	0.8517	86.15	84.21	91.92	90.00
Xception	0.4454	42.31	47.01	76.15	64.87
ResNet18	0.8594	84.62	87.30	93.85	90.77
MobileNetV2	0.8712	88.46	85.82	92.69	91.28
InceptionV3	0.7094	72.31	69.63	84.23	80.26
NasNetMobile	0.7405	82.31	67.30	80.00	80.77
E1	0.8651	83.85	89.34	95.00	91.28
E2	0.8203	80.77	83.33	91.92	88.21
E3	0.8271	84.62	80.88	90.00	88.21
Proposed	0.9112	90.77	91.47	95.77	94.10

		Actual		Actual	
		Positive	Negative	Positive	Negative
Predicted	Positive	396	1	195	4
	Negative	4	199	5	196

a

b

Fig. 25. Confusion matrix of proposed method for mini-DDSM dataset: (a) Abnormality identification (b) Malignancy identification.

		Actual		Actual	
		Positive	Negative	Positive	Negative
Predicted	Positive	255	7	124	8
	Negative	5	123	6	122

a

b

Fig. 26. Confusion matrix of proposed method for BUSI dataset: (a) Abnormality identification (b) Malignancy identification.

		Actual	
		Positive	Negative
Predicted	Positive	97	2
	Negative	3	98

Fig. 27. Confusion matrix of proposed method for BUSI dataset.

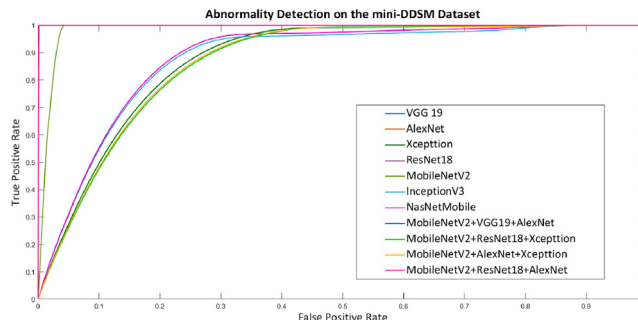


Fig. 28. ROC curve to detect abnormality on mini-DDSM for 6th fold.

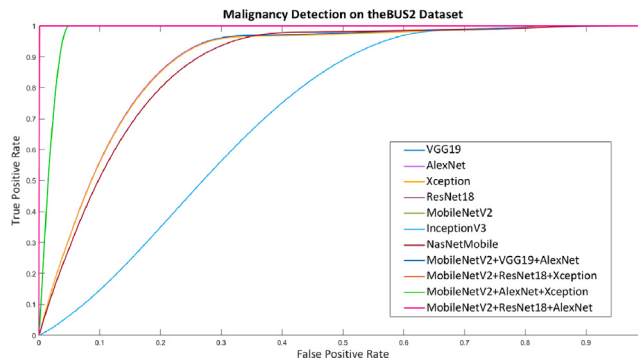


Fig. 29. ROC curve to detect malignancy on mini-DDSM for 6th fold.

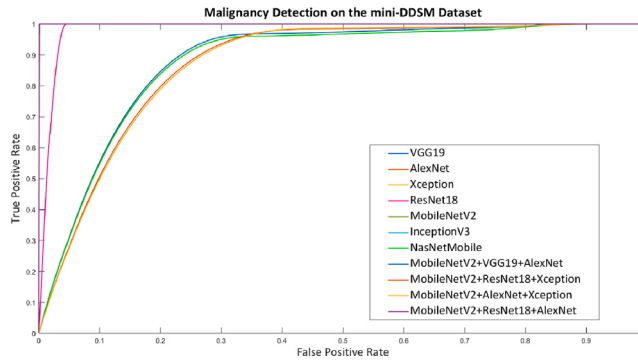


Fig. 30. ROC curve to detect abnormality on BUSI for 6th fold.

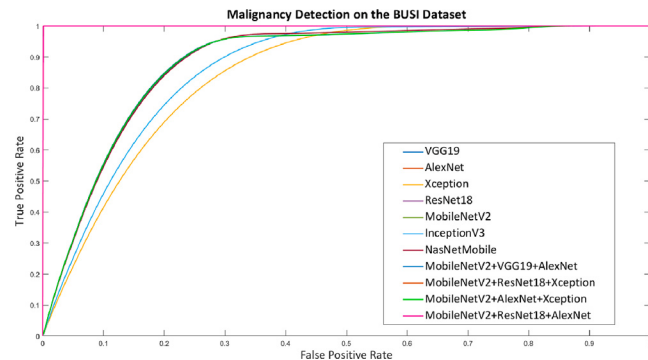


Fig. 31. ROC curve to detect malignancy on BUSI for 6th fold.

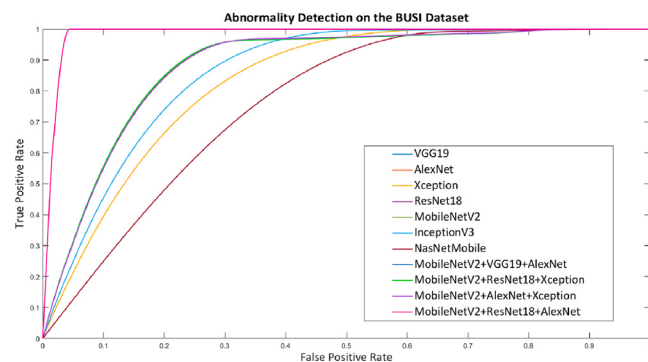


Fig. 32. ROC curve to detect malignancy on BUS2 for 6th fold.

Table 14
Dataset-wise comparison of elapsed time (in s).

Method	mini-DDSM	BUSI	BUS2
Vgg19	0.094	0.162	0.067
AlexNet	0.015	0.037	0.014
Xception	0.342	0.602	0.326
ResNet18	0.180	0.040	0.015
MobileNetV2	0.064	0.118	0.059
InceptionV3	0.132	0.239	0.115
NasNetMobile	0.367	0.654	0.325
E1	0.188	0.322	0.155
E2	0.439	0.853	0.415
E3	0.436	0.772	0.414
Proposed	0.112	0.210	0.103

approaches given in **Table 14**. ResNet and MobileNetV2 come after AlexNet as the second and third computationally efficient networks. However, it is faster than VGG19, Xception, InceptionV3, NasNetMobile and the other ensemble classifiers. Though the proposed method is more computationally complex than AlexNet, MobileNetV2, and ResNet18, its classification performance makes it a preferred approach over other techniques.

Tables 15 through 17 demonstrate a comparative performance analysis with existing works regarding different performance measures for mini-DDSM, BUSI, and BUS2 datasets, respectively. These tables show that the proposed ensemble method exhibits higher accuracy and precision than the existing literature mentioned.

5.1. Significance of proposed work

In this section, we have presented a brief discussion on the significance of the proposed breast cancer framework which may motivate others to do research on this platform. As the proposed technique integrates the benefits of AlexNet, ResNet18, and MobileNetV2 it delivers an admirable performance.

is not possible. From these tables it is found that the performance of benign is relatively poor than other two classes in both the datasets. It occurs because in benign identification malignant and normal images are treated as one class and benign as other class. It is comparatively difficult for the system for accurate prediction.

Table 14 represents the testing time per image in seconds for both abnormality detection and malignancy detection in all three modalities. The table conveys that AlexNet is the fastest Network among all the

Table 15
Comparative performance analysis with recent works on DDSM database.

Existing methods	Year	Sensitivity (%)	Specificity (%)	Accuracy (%)	Precision (%)
[21]	2017	83.30	79.80	80.02	–
[5]	2019	–	–	82.02	–
[23]	2019	95.60	95.36	94.55	–
[38]	2019	–	96.00	97.00	–
[24]	2020	87.30	84.00	85.71	85.7
[25]	2020	91.00	–	88.00	85.00
[17]	2021	84.1	93.00	88.70	91.70
[26]	2021	97.00	98.00	96.00	–
[7]	2022	97.72	88.21	90.68	–
[39]	2023	91.54	91.54	91.54	0.9154
Proposed	–	98.00	97.50	97.75	97.51

Table 16
Comparative performance analysis with recent works on BUSI database.

Existing methods	Year	Specificity (%)	Accuracy (%)	Sensitivity (%)	Precision (%)
[18]	2018	–	88.76	–	–
[22]	2019	–	78.00	–	–
[27]	2021	89.70	92.30	–	–
[7]	2022	85.26	89.34	93.14	–
Proposed	–	93.85	94.62	95.38	93.94

Table 17
Comparative performance analysis with recent works on BUS2 dataset.

Method	F1 Score	Sensitivity (%)	Precision (%)	Specificity (%)	Accuracy (%)
[40]	0.9664	97.30	96.00	94.12	96.00
[41]	0.9527	94.00	96.57	95.00	94.40
[42]	–	97.35	98.00	96.97	97.20
Proposed	0.9749	97.00	97.98	98.00	97.50

In the mini-DDSM dataset, for abnormality detection, ResNet18 delivers superior performance in terms of sensitivity since the overall false negative is less than others, as seen in Table 4. On the other hand, MobileNetV2 exhibits better performance than others in terms of precision and specificity, as it yields comparatively fewer false positives. In malignancy detection, ResNet18 gives the least false negative resulting in better sensitivity, whereas both ResNet and MobileNetV2 yield fewer false positives and hence exhibit better precision and specificity than others, as observed in Table 5. In both abnormality and malignancy detection, overall FP and FN values are less for AlexNet than VGG19 and Xception using the mini-DDSM dataset.

In the BUSI dataset, to detect an abnormality, AlexNet beats other base classifiers in terms of all the performance measures as the overall false positive and false negative value is less. After AlexNet, two other systems, ResNet and MobileNetV2, also exhibit very good classification performance, as observed in Table 6. Since ResNet18 yields fewer false positives, it gives better precision and specificity, whereas MobileNetV2 gives better sensitivity as its overall false negative is less. For malignancy detection, AlexNet yields fewer False Negatives that result in the best sensitivity among all the base classifiers, as seen in Table 7. ResNet18 exhibits the least number of FP, resulting in better precision and specificity. In BUS2, MobileNetV2 yields the least false positive, whereas ResNet yields the minimum false. Hence, the combination of both ResNet18 and MobileNetV2 with AlexNet shows promising performance.

Efficient transfer learning models can be combined with meta-heuristic algorithms [43,44] to improve the performance further. Similarly, there are various opportunities for additional performance enhancement. Some prospective scopes are shown below.

5.2. Future directions

- Some competent variants of conventional transfer learning techniques can be utilized to build more effective ensemble approaches.

- By combining the beneficial characteristics of sparse learning with transfer learning, more efficient systems may be constructed for lesser amount of data.
- Efficient breast cancer detection system can be developed by combining the advantages of transfer learning and meta-heuristic algorithms.
- The presented approaches have the potential to be used in various computer vision domain and mobile healthcare.

The experimental results depict the proposed ensemble approach outperforms others with the best performances. However, for very few images, if any two models give a false prediction, then the overall prediction will be wrong. Though it rarely occurs, the performance can be improved further by using more efficient models as fundamental classifiers, which is one of our future research directions. The overall false positive and false negative value is less for AlexNet, MobileNetV2, and ResNet than VGG19, InceptionV3, NasNetMobile, and Xception in both abnormality and malignancy detection in mini-DDSM, BUSI, and BUS2 datasets. Since the proposed method is an ensemble of AlexNet, MobileNetV2, and ResNet, they take advantage of all three methods to minimize false positives and false negatives. Thus, the performance of the suggested technique is also improved, and it achieves the best results.

6. Conclusion

The experimental results depict the proposed ensemble approach outperforms others with the best performances. However, if any two models give a false prediction for very few images, then the overall prediction will be wrong. Though it rarely occurs, the performance can be improved further by using more efficient models as fundamental classifiers, which is one of our future research directions. The overall false positive and false negative value is less for AlexNet, MobileNetV2, and ResNet than VGG19, InceptionV3, NasNetMobile, and Xception.

Since the proposed method is an ensemble of AlexNet, MobileNetV2, and ResNet, they take advantage of all three methods to minimize false positives and false negatives. The proposed technique exhibits higher classification performance across three different datasets, according to the experimental results. It obtains an accuracy of 99.17% for abnormality detection and 97.75% for malignancy detection in the mini-DDSM dataset. Similar accuracy rates of 96.92% and 94.62% for abnormality and cancer detection are attained on the BUSI ultrasonography dataset. Notably, the model achieves an accuracy of 97.50% on the BUS2 ultrasonography dataset, doing remarkably well. These findings demonstrate the model's adaptability and dependability, which makes it acceptable for breast cancer diagnosis in multimodal datasets.

CRediT authorship contribution statement

Adyasha Sahu: Conceptualization, Methodology, Software, Validation, Writing – original draft. **Pradeep Kumar Das:** Supervision, Investigation, Suggestions for the improvement of the manuscript. **Sukadev Meher:** Supervision, Investigation, Suggestions for the improvement of the manuscript.

Declaration of competing interest

The authors declare that they have no known competing financial interests or personal relationships that could have appeared to influence the work reported in this paper.

Data availability

The authors do not have permission to share data.

References

- [1] A. Sahu, P.K. Das, S. Meher, High accuracy hybrid CNN classifiers for breast cancer detection using mammogram and ultrasound datasets, *Biomed. Signal Process. Control* 80 (2023) 104292.
- [2] X. Shu, L. Zhang, Z. Wang, Q. Lv, Z. Yi, Deep neural networks with region-based pooling structures for mammographic image classification, *IEEE Trans. Med. Imaging* 39 (6) (2020) 2246–2255.
- [3] V.S. Gnanasekaran, S. Joypaul, P.M. Sundaram, D.D. Chairman, Deep learning algorithm for breast masses classification in mammograms, *IET Image Process.* 14 (12) (2020) 2860–2868.
- [4] V.K. Singh, H.A. Rashwan, S. Romani, F. Akram, N. Pandey, M.M.K. Sarker, A. Saleh, M. Arenas, M. Arquez, D. Puig, et al., Breast tumor segmentation and shape classification in mammograms using generative adversarial and convolutional neural network, *Expert Syst. Appl.* 139 (2020) 112855.
- [5] L. Sun, J. Wang, Z. Hu, Y. Xu, Z. Cui, Multi-view convolutional neural networks for mammographic image classification, *IEEE Access* 7 (2019) 126273–126282.
- [6] P.K. Das, S. Meher, An efficient deep convolutional neural network based detection and classification of acute lymphoblastic leukemia, *Expert Syst. Appl.* (2021) 115311.
- [7] D. Muduli, R. Dash, B. Majhi, Automated diagnosis of breast cancer using multimodal datasets: A deep convolution neural network based approach, *Biomed. Signal Process. Control* 71 (2022) 102825.
- [8] P.K. Das, S. Meher, R. Panda, A. Abraham, A review of automated methods for the detection of sickle cell disease, *IEEE Rev. Biomed. Eng.* 13 (2019) 309–324.
- [9] S.I. Khan, R.B. Pachori, Derived vectorcardiogram based automated detection of posterior myocardial infarction using FBSE-EWT technique, *Biomed. Signal Process. Control* 70 (2021) 103051.
- [10] P.K. Das, S. Meher, Transfer learning-based automatic detection of acute lymphocytic leukemia, in: 2021 National Conference on Communications, NCC, IEEE, 2021, pp. 1–6.
- [11] P.K. Das, B. Nayak, S. Meher, A lightweight deep learning system for automatic detection of blood cancer, *Measurement* (2022) 110762.
- [12] P.K. Das, A. Pradhan, S. Meher, Detection of acute lymphoblastic leukemia using machine learning techniques, in: Machine Learning, Deep Learning and Computational Intelligence for Wireless Communication, Springer, 2021, pp. 425–437.
- [13] P.K. Das, B. Sahoo, S. Meher, An efficient detection and classification of acute leukemia using transfer learning and orthogonal softmax layer-based model, *IEEE/ACM Trans. Comput. Biol. Bioinform.* (2023).
- [14] I. Paul, A. Sahu, P.K. Das, S. Meher, Deep convolutional neural network-based automatic detection of brain tumour, in: 2023 2nd International Conference for Innovation in Technology, INOCON, 2023, pp. 1–6.
- [15] M. Abdar, M. Zomorodi-Moghadam, X. Zhou, R. Gururajan, X. Tao, P.D. Barua, R. Gururajan, A new nested ensemble technique for automated diagnosis of breast cancer, *Pattern Recognit. Lett.* 132 (2020) 123–131.
- [16] M. Abdar, V. Makarenkov, CWV-BANN-SVM ensemble learning classifier for an accurate diagnosis of breast cancer, *Measurement* 146 (2019) 557–570.
- [17] S. Shakeel, G. Raja, Classification of breast cancer from mammogram images using deep convolution neural networks, in: 2021 International Bhurban Conference on Applied Sciences and Technologies, IBCAST, IEEE, 2021, pp. 595–599.
- [18] C.-Y. Lee, G.-L. Chen, Z.-X. Zhang, Y.-H. Chou, C.-C. Hsu, Is intensity inhomogeneity correction useful for classification of breast cancer in sonograms using deep neural network, *J. Healthcare Eng.* 2018 (2018).
- [19] S. Maqsood, R. Damaševičius, R. Maskeliūnas, TTCNN: A breast cancer detection and classification towards computer-aided diagnosis using digital mammography in early stages, *Appl. Sci.* 12 (7) (2022) 3273.
- [20] D.A. Zebari, D.A. Ibrahim, D.Q. Zeebaree, H. Haron, M.S. Salih, R. Damaševičius, M.A. Mohammed, Systematic review of computing approaches for breast cancer detection based computer aided diagnosis using mammogram images, *Appl. Artif. Intell.* 35 (15) (2021) 2157–2203.
- [21] B. Swiderski, S. Osowski, J. Kurek, M. Kruk, I. Lugowska, P. Rutkowski, W. Barhoumi, Novel methods of image description and ensemble of classifiers in application to mammogram analysis, *Expert Syst. Appl.* 81 (2017) 67–78.
- [22] W. Al-Dhabayani, M. Gomaa, H. Khaled, F. Aly, Deep learning approaches for data augmentation and classification of breast masses using ultrasound images, *Int. J. Adv. Comput. Sci. Appl.* 10 (5) (2019) 1–11.
- [23] H. Li, S. Zhuang, D.-a. Li, J. Zhao, Y. Ma, Benign and malignant classification of mammogram images based on deep learning, *Biomed. Signal Process. Control* 51 (2019) 347–354.
- [24] A.S.A. Rahman, S.B. Belhaouari, A. Bouzerdoum, H. Baali, T. Alam, A.M. Eldaraa, Breast mass tumor classification using deep learning, in: 2020 IEEE International Conference on Informatics, IoT, and Enabling Technologies, ICIoT, IEEE, 2020, pp. 271–276.
- [25] R. Arora, P.K. Rai, B. Raman, Deep feature-based automatic classification of mammograms, *Med. Biol. Eng. Comput.* 58 (6) (2020) 1199–1211.
- [26] S.J. Malebary, A. Hashmi, Automated breast mass classification system using deep learning and ensemble learning in digital mammogram, *IEEE Access* 9 (2021) 55312–55328.
- [27] M. Byra, Breast mass classification with transfer learning based on scaling of deep representations, *Biomed. Signal Process. Control* 69 (2021) 102828.
- [28] Z. Zhuang, Z. Yang, A.N.J. Raj, C. Wei, P. Jin, S. Zhuang, Breast ultrasound tumor image classification using image decomposition and fusion based on adaptive multi-model spatial feature fusion, *Comput. Methods Programs Biomed.* 208 (2021) 106221.
- [29] D.A. Zebari, D.A. Ibrahim, D.Q. Zeebaree, M.A. Mohammed, H. Haron, N.A. Zebari, R. Damaševičius, R. Maskeliūnas, Breast cancer detection using mammogram images with improved multi-fractal dimension approach and feature fusion, *Appl. Sci.* 11 (24) (2021) 12122.
- [30] T. Meraj, W. Alosaimi, B. Alouff, H.T. Rauf, S.A. Kumar, R. Damaševičius, H. Alyami, A quantization assisted U-net study with ICA and deep features fusion for breast cancer identification using ultrasonic data, *PeerJ Comput. Sci.* 7 (2021) e805.
- [31] P.K. Das, S. Meher, R. Panda, A. Abraham, An efficient blood-cell segmentation for the detection of hematological disorders, *IEEE Trans. Cybern.* 12 (2022) 10615–10626.
- [32] A. Krizhevsky, I. Sutskever, G.E. Hinton, Imagenet classification with deep convolutional neural networks, in: Advances in Neural Information Processing Systems, 2012, pp. 1097–1105.
- [33] K. He, X. Zhang, S. Ren, J. Sun, Deep residual learning for image recognition, in: Proceedings of the IEEE Conference on Computer Vision and Pattern Recognition, 2016, pp. 770–778.
- [34] M. Sandler, A. Howard, M. Zhu, A. Zhmoginov, L.-C. Chen, Mobilenetv2: Inverted residuals and linear bottlenecks, in: Proceedings of the IEEE Conference on Computer Vision and Pattern Recognition, 2018, pp. 4510–4520.
- [35] C.D. Lekamge, F. Afzal, E. Westerberg, A. Cheddad, Mini-DDSM: Mammography-based automatic age estimation, 2020, arXiv preprint arXiv:2010.00494.
- [36] W. Al-Dhabayani, M. Gomaa, H. Khaled, A. Fahmy, Dataset of breast ultrasound images, *Data brief* 28 (2020) 104863.
- [37] P.S. Rodrigues, Breast ultrasound image, Mendeley Data 1 (2017).
- [38] N. Safdarian, M. Hedayezadeh, Detection and classification of breast cancer in mammography images using pattern recognition methods, *Multidisc. Cancer Invest.* 3 (4) (2019) 13–24.
- [39] A. Sahu, P.K. Das, S. Meher, R. Panda, A. Abraham, An efficient deep learning-based breast cancer detection scheme with small datasets, in: Intelligent Systems Design and Applications: 22nd International Conference on Intelligent Systems Design and Applications (ISDA 2022) Held December 12-14, 2022-Volume 4, Vol. 717, Springer Nature, 2023, p. 39.
- [40] S.M. Kabir, A. Shihavuddin, M.S. Tanveer, M.I.H. Bhuiyan, Parametric image-based breast tumor classification using convolutional neural network in the contourlet transform domain, in: 2020 11th International Conference on Electrical and Computer Engineering, ICECE, IEEE, 2020, pp. 439–442.

- [41] P. Acevedo, M. Vazquez, Classification of tumors in breast echography using a SVM algorithm, in: 2019 International Conference on Computational Science and Computational Intelligence, CSCI, IEEE, 2019, pp. 686–689.
- [42] S. Mahmud Kabir, S. Tanveer, A. Shihavuddin, M. Imamul Hassan Bhuiyan, et al., Weighted contourlet parametric (WCP) feature based breast tumor classification from B-mode ultrasound image, 2021, arXiv e-prints, arXiv-2102.
- [43] S.M. Qaisar, S.I. Khan, D. Dallet, R. Tadeusiewicz, P. Pławiak, Signal-piloted processing metaheuristic optimization and wavelet decomposition based elucidation of arrhythmia for mobile healthcare, *Biocybern. Biomed. Eng.* 42 (2) (2022) 681–694.
- [44] S.I. Khan, R.B. Pachori, Automated classification of lung sound signals based on empirical mode decomposition, *Expert Syst. Appl.* 184 (2021) 115456.